International Journal of Architectural, Civil and Construction Sciences
ISSN: 2415-1734
Vol:7, No:9, 2013

Numerical Simulations of Flood and Inundation in Jobaru River Basin Using Laser Profiler Data

Hiroto Nakashima, Toshihiro Morita, and Koichiro Ohgushi

***Abstract*—**Laser Profiler (LP) data from aerial laser surveys have been increasingly used as topographical inputs to numerical simulations of flooding and inundation in river basins. LP data has great potential for reproducing topography, but its effective usage has not yet been fully established. In this study, flooding and inundation are simulated numerically using LP data for the Jobaru River basin of Japan's Saga Plain. The analysis shows that the topography is reproduced satisfactorily in the computational domain with urban and agricultural areas requiring different grid sizes. A 2-D numerical simulation shows that flood flow behavior changes as grid size is varied.

***Keywords*—**LP data, numerical simulation, topological analysis, mesh size.

I. Introduction

IN recent years, there has been much discussion of unexpectedly large, frequent floods caused by abnormal weather, and of possible countermeasures to mitigate them. One of these countermeasures is the creation of predicted inundation maps based on numerical simulations of flooding and inundation. Laser Profiler data obtained from aerial laser surveys are used to create the topographical inputs necessary for the numerical simulations. Although detailed topography must be reproduced employing LP data to ensure appropriate modeling of existing conditions, its effective use has not yet been fully established.

An unstructured numerical grid produces a finer topography than a structured one can. To utilize LP data with maximum efficiency when performing Delaunay triangulation (a popular method for generating unstructured grids), a large number of numerical grids must be used. This, however, vastly increases simulations' computation time. Thus, we need a balance between having highly accurate, finely reproduced topography and limiting the number of numerical grids to ease the computational burden.

In this study, it simulated flooding and inundation numerically using LP data for the Jobaru River basin in Japan's Saga Plain. It compares the behavior of flood flows that result when different grid sizes are used to reproduce the basin's topography.

Hiroto Nakashima is graduate student in the Department of Civil Engineering and Architecture, Faculty of Science and Engineering, Saga University, Japan (e-mail: 12577018@ edu.cc.saga-u.ac.jp).
Toshihiro Morita is doctoral student in the Course of Circulation Society Systems Researches, Department of Create Technology Systems, Saga University, Japan (e-mail: 12577018@ edu.cc.saga-u.ac.jp).
Koichiro Ohgushi is professor in the Department of Civil Engineering and Architecture, Faculty of Science and Engineering, Saga University, Japan (e-mail: ohgushik@cc.saga-u.ac.jp).

II. Jobaru River

A. Overview

A plan view of the Jobaru River is shown in Fig. 1. It originates at Mt. Seburi, joins the Sagae River, and then flows into the Chikugo River that goes to the Ariake Sea. The catchment area of the Jobaru River is about 64.4 km^2, and its trunk watercourse is about 31.9 km long.

The 2006 riparian work plan for the Chikugo River basin is set at a target maximum discharge of 540 m^3/s at Hidekibashi Station, which includes the storage efficiency of the Jobaru River dam whose construction has not be decided yet. Considering controversy that arose over the dam's construction, we set the target discharge in the river channel at 330 m^3/s.

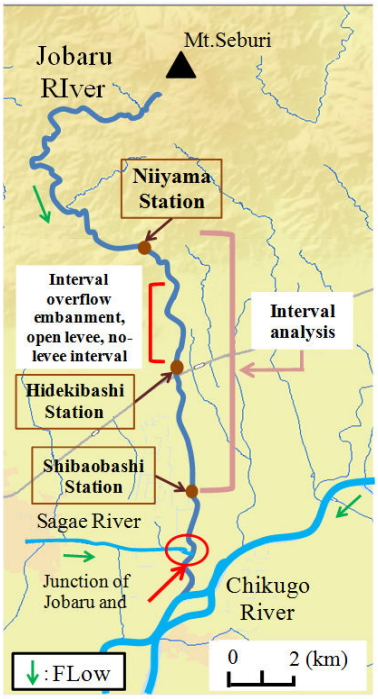

Fig. 1 Plan view of the Jobaru River basin

B. River Basin Management

Along the Jobaru River, traditional flood control facilities such as overflow embankments (called "Nokoshi") and open levees (called "Kasumi-tei") have existed for about 400 years. These facilities manage flooding that cannot be controlled in the river channel alone.

A sectional view of a Nokoshi is shown in Fig. 2. Water overflows into a retarding basin and is controlled by an

auxiliary levee in a residential area (called a "Mizuuke-tei") to protect neighboring villages from flood disaster.

An "open levee" is a type of discontinuous levee often used in steep streams. If the water level in a landside area rises higher than the level of the overflow embankment, the water begins to move as one body with the main river flow [1].

There are two levee intervals without banks on the Jobaru River. In these stretches the water is stored directly in the neighborhood retarding basin.

Fig. 3 shows a plan view of the Jobaru River basin overflow system. There are four open levees, five Nokoshis, and two no-levee intervals along the Jobaru River.

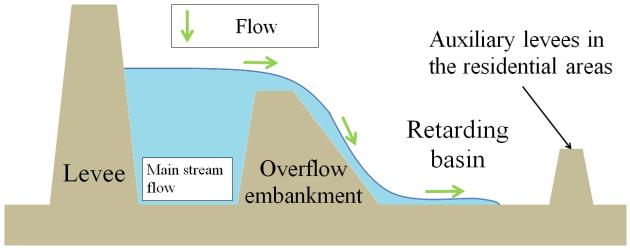

Fig. 2 Sectional view of Nokoshi overflow embankment

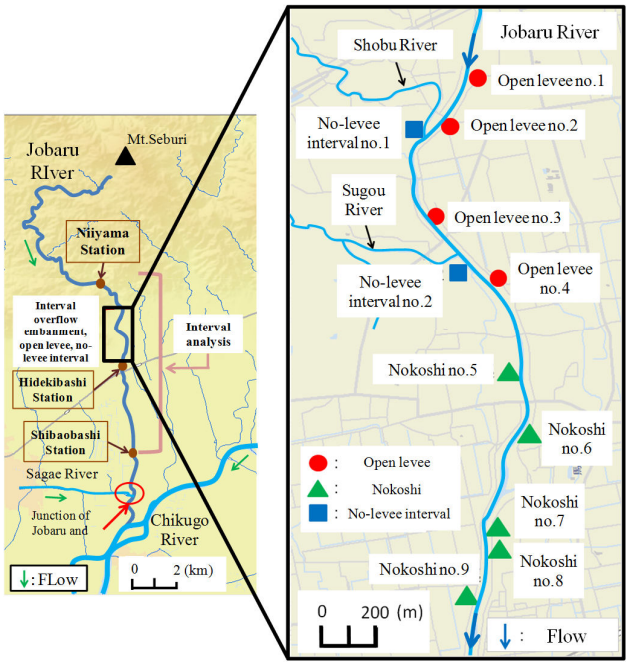

Fig. 3 Plan view of Jobaru River basin overflow system

C. Jobaru River Basin Summary

After flood disasters in 1949 and 1953, subsidy projects were implemented from 1953 to 1961 in the Jobaru River basin. Fig. 4 shows plan views of the Jobaru River before and after the disaster subsidy projects were completed. The Jobaru River was widened and some Nokoshis and open levees were moved. An auxiliary levee in a landside area was removed to allow use of arable land, and other changes were made. The land use changed considerably. As a result of this work, there are presently Nokoshis and open levees that act as overflow levees without retarding basins.

Fig. 4 Plan views of the Jobaru River before (left) and after (right) construction of disaster subsidy projects

III. Simulation Methods

A. Generation of Unstructured Grids [2]

The Delaunay triangulation method and the advancing front method are two major methods for creating unstructured grids. The advancing front method sets new nodes inside of boundaries one by one within a study domain (for example, a neighborhood can constitute a boundary if it limits to a 2-D domain), generating triangle or quadrangles that satisfy geometric conditions, ultimately filling the domain. This method has an advantage in that it is only necessary to specify nodes on the boundary. However, the resulting element form has a fault in that it only achieves local optimization.

The Delaunay triangulation method divides a domain into triangles in the 2-D case into tetrahedrons in the 3-D case for an arbitrarily set up contact group. A circle (sphere in the 3-D case) must be circumscribed about all the elements obtained by this method. Other points of contact are known to exist that are not inside the circle (sphere). This agrees with the element form required for finite element methods used widely in numerical analysis. The geometric character of the Delaunay triangulation is used as the foundation of many element breakdown methods. However, it also has some faults, as it is not applicable as-is to convex domains, and all nodes must be given.

In this study, we generated unstructured grids using the Delaunay triangulation method. The maximum grid areas were set to 50 m^2, 40 m^2, 30 m^2, 20 m^2, 10 m^2, 5 m^2 and 4 m^2.

B. Study Area

Fig. 5 shows the study area, which lies on the left bank side of the landside area surrounding open levee no. 1 on the Jobaru River. As mentioned above, there are Nokoshis and open levees that act as overflow levees without retarding basins at present. Therefore, the behavior of inundation flows in the landside area is not yet clear. Moreover, open levee no. 1 has the widest weir width of the open levees, so it is thought to allow maximum water flow. Table I [3] shows the widths of all the discontinuous levees along the Jobaru River. At present, the city is distributed in the southeast area of open levee no. 1, presenting the risk of disaster caused by overflow from the open levee. Therefore, we must assume flooding in the study area from a disaster prevention point of view.

TABLE I
WIDTHS OF ALL DISCONTINUOUS LEVEES ALONG THE JOBARU RIVER [3]

Location	Weir width (m)
No-levee interval no. 1	144.2
No-levee interval no. 2	94.2
Open levee no. 1	50.0
Open levee no. 2	21.0
Open levee no. 3	14.0
Open levee no. 4	25.0
Nokoshi no.5	14.0
Nokoshi no. 6	39.0
Nokoshi no. 7	22.0
Nokoshi no. 8	24.0
Nokoshi no. 9	22.0

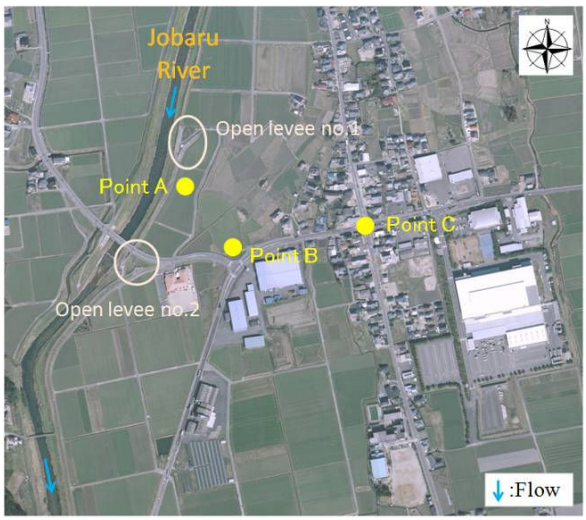

Fig. 5 Land use of landside area near open levee no. 1

TABLE II
LP DATA SPECIFICATIONS

Item	Specification
VER (type of profiler)	ALS50
Observed altitude	4600 feet
Flight height above the ground	200 km/h
Pulse rate	67.5 kHz
Angle of scan	30°
Scan times	40 Hz
Along-track direction average measurement density	~ 1.4 m
Cross-track direction average measurement density	~ 1.4 m

B. Laser Profiler (LP) data [4]

The LP data are topographical data measured by aerial laser surveys. The aerial survey is a survey technology that can obtain 3-D data by analyzing laser pulses shot toward the ground from an aviation laser scanner carried in an airplane or helicopter that reflect off the ground and return. The accuracy (standard deviation) of the original data is less than 25cm horizontally.

Table II shows the specifications of the observed LP data. The data were obtained on 28 December 2005 and 11 January 2006. Our numerical simulations use the original LP data without removing structures such as houses, buildings, etc.

C.2-D Inundation Simulations

In this study, flooding and inundation are analyzed using different maximum grid sizes in the study area. Fig. 5 shows three typical observation points: A (an agricultural area), B (where water flow is stagnated by the road embankment), and C (an urban intersection). The optimum solution is examined from the numerical simulation.

The fundamental equation for 2-D simulations is:

$$\frac{\partial h}{\partial t}+\frac{\partial h\bar{u}}{\partial x}+\frac{\partial h\bar{v}}{\partial y}=0 \quad (1)$$

$$\frac{\partial h\bar{u}}{\partial t}+\frac{\partial h\bar{u}^{2}}{\partial x}+\frac{\partial h\overline{vu}}{\partial y}=-gh\frac{\partial \eta}{\partial x}-\frac{\tau_{bx}}{\rho_0} \quad (2)$$

$$\frac{\partial h\bar{v}}{\partial t}+\frac{\partial h\overline{uv}}{\partial x}+\frac{\partial h\bar{v}^{2}}{\partial y}=-gh\frac{\partial \eta}{\partial y}-\frac{\tau_{by}}{\rho_0} \quad (3)$$

where h is water depth, t is time, g is gravitational acceleration, ρ_0 is density, $\bar{u}$ and $\bar{v}$ are depth-averaged velocity components, η is water level, and τ_{bx} and τ_{by} are bottom-stress components.

As a boundary condition, it set an overflow discharge at open levee no. 1 and open levee no. 2. It generated the discharge for the simulation based on rain that occurred on 11-14 July 2010. The main channel's flood flow was simulated using 1-D flow analysis with water overflowing through the open levees on the Jobaru River [5].

IV. SIMULATION RESULTS AND CONSIDERATIONS

A. Topography Reproducibility Differences Due to Grid Size

The topography as interpolated by two different grid sizes (maximum 50 m^2 and maximum 5 m^2) is shown in Fig. 6. The 5m^2 grid reproduced roads, paths between rice fields and houses more accurately but the 50m^2 grid captured much of the area's impalpable topography.

The absolute values of the differences between the two grids were converted to a black and white scale, as shown in Fig. 7. There are many differences in the boundaries of houses and roads, but few in agricultural areas. Thus, areas with more varied topography are more greatly influenced by maximum grid size.

B. 2-D Flood and Inundation Simulation Results and Considerations

Figs. 8 and 9 show the simulated inundation levels 10min and 30min after the water starts to overflow from the open levee. Ten minutes after the overflow starts, the topography with the 50 m^2 maximum grid area affects flow further downstream than the 5 m^2 grid topography. Thirty minutes after the overflows starts, the 50 m^2 grid topography is immersed by the water, making undulations in agricultural areas. The inundation has progressed quickly. However, with the 5 m^2 grid, the undulation in agricultural areas is still seen clearly, so the inundation flow is reproduced appropriately.

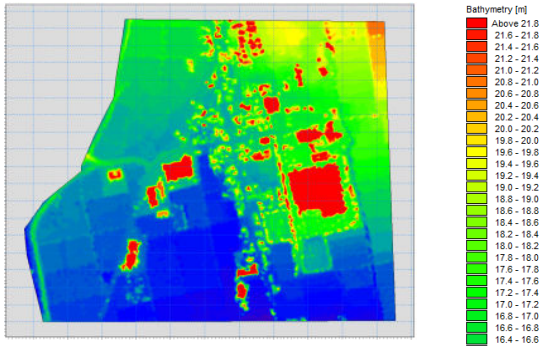

The case of 50 m^2 maximum grid area

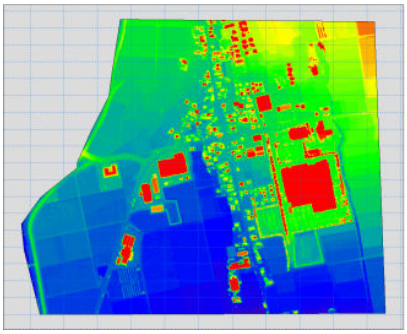

The case of 5m^2 maximum grid area

Fig. 6 Comparison of topography with 50 m^2 and 5 m^2 maximum grid areas

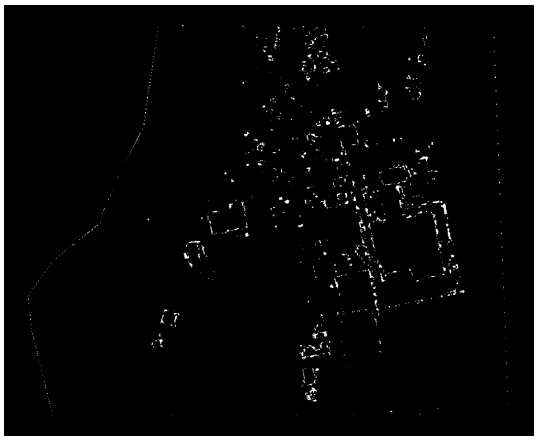

Fig. 7 Absolute values of topography variation between 50 m^2 and 5 m^2 maximum area grids, displayed with black showing small differences to white showing large differences

Temporal changes of simulated water depth at point A, an agricultural area, produced using different maximum grid areas are shown in Fig. 10. At t = 7:55 min, the water depths for topographies with maximum grid areas of 20 m^2 to 50 m^2 vary considerably, but those for 4 m^2 and 5 m^2 grids agree to within 0.01 m. At t = 8:09, the 20 m^2 to 50 m^2 grids agree. The water depth reached as time passes increases as the maximum grid area decreases. The depth for the 4 m^2 grid is 0.1 m higher than for the 50 m^2 grid. At t = 8:27, all cases show the depth to be changing in the same way.

Fig. 11 shows temporal changes of water depth with different maximum grid areas at point B, where the water flow is stagnated by the road embankment. At t = 8:04, the 10 m^2 to 50 m^2 grid topographies produce different modeled water depths while the 4 m2 and 5 m2 grid topographies' depths agree. From t = 8:03, the 20 m^2 to 50 m^2 grid topographies produce different modeled depths, but the 4 m^2, 5 m^2, and 10 m^2 topographies produce nearly identical water depths.

Temporal changes of water depth at point C, an urban intersection, simulated using different maximum grid areas are shown in Fig. 12. Every grid size produces different temporal changes of water depth. Moreover, since the inundation flows reached their boundaries and were reflected, the examination cannot be completed by t = 8:35.

The times at which the inundation flow arrives at the boundary differ. This is thought to be caused by variations in the behavior of the inundation flows produced using topographies having different maximum grid areas.

At points A and B, the behavior of the inundation flows are very similar, leading to the conclusion that the actual topography is reproduced appropriately using a maximum grid area of 4 m^2.

At point C, however, the 4 m^2 and 5 m^2 grid topographies produce different temporal water depth changes. Because there are many houses and buildings, there may be large changes in altitude at point C. The maximum grid area should be made still smaller in vicinities with dense structures to better model the actual conditions.

The differences arising from maximum grid size diminished as water depth increased at point A. Since point A is farmland with little altitude variation, it appears that the influence of small-scale features like ground surface undulations decreases as water depth increases.

From the results obtained in the above, the selection of an appropriate grid size area, while considering the structures in the studied area to simulate the behavior of inundation flow, was made.

V. Conclusion

This study revealed the following:

1) Topographical analysis shows that differences in the calculation grid area affect topographic reproduction more in urban areas than in agricultural areas.
2) The 2-D numerical simulation shows that the maximum grid area affects the simulated inundation flow behavior and changes of water depth measured at individual points.
3) At points A and B, areas where there is little altitude variation, topographies with maximum grid areas of 4 m^2 and 5 m^2 produce simulated depths that agree with each other. At point C, however, where the altitude varies more, the 4 m^2 and 5 m^2 grids produced different temporal depth changes.

4) We found that time at which inundation flows arrive at given locations differs as the maximum grid area changes.

ACKNOWLEDGMENTS

This work was supported by JSPS KAKENHI, 23310128, Grant-in-Aid for Scientific Research (B). The Ministry of Land, Infrastructure, Transport and Tourism provided the LP and hydraulic data. Dr. Tezuka, assistant professor in the Department of Civil Engineering at Nihon University devotedly supported our study.

The case of 50 m^2 maximum grid area

The case of 5 m^2 maximum grid area

Fig. 8 Flood flow behavior 10 minutes after overflow starts

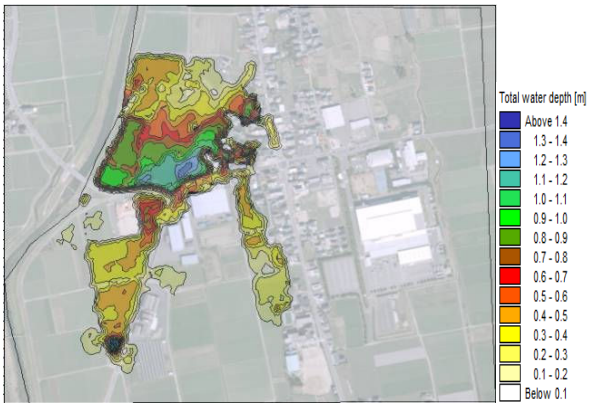

The case of 50 m^2 maximum grid area

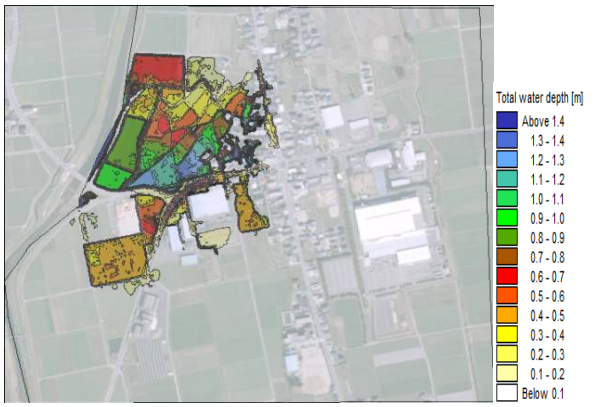

The case of 5 m^2 maximum grid area

Fig. 9 Flood flow behavior 30 minutes after overflow starts

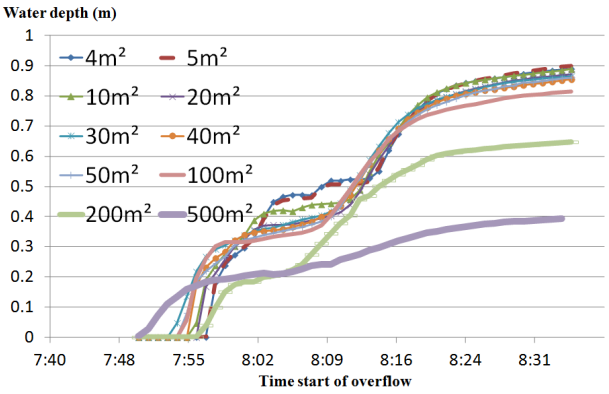

Fig. 10 Temporal changes of water depth with different grid areas at point A

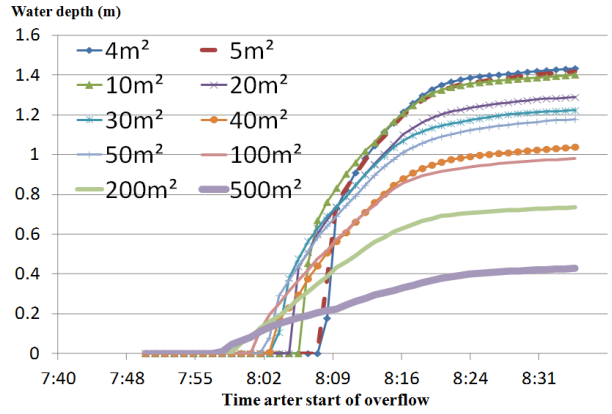

Fig. 11 Temporal changes of water depth with different grid areas at point B

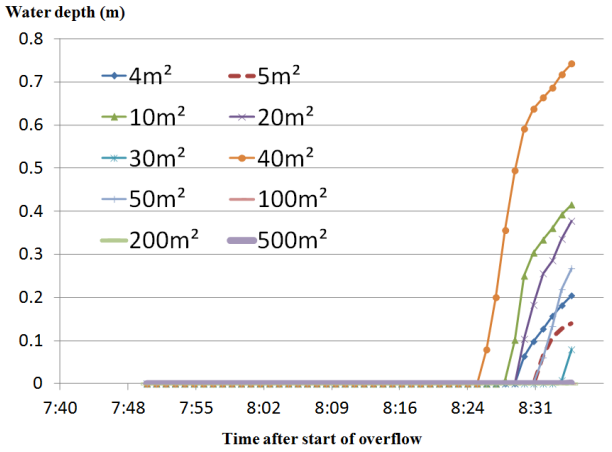

Fig. 12 Temporal changes of water depth with different grid areas at point C

REFERENCES

[1] Y.Takahashi, *A new edition River Engineering*, p.207, 2008
[2] T. Taniguti, *Automatic mesh generation for FEM –using Delaunay triangulation-*, MORIKITA PUBLISHING, 1992.
[3] T. Tanabe, T. Okuma, A Study on the Roles Effect of "NOKOSHI" on the Jobaru-River Basin Example of Flood Control that Allows Overflowing and its Future Possibility, History of civil engineering, Vol.21, p.p.147-158, May, 2001.
[4] The Geographical Survey Institute of MLIT, The digital elevation model (DEM) creation manual by aerial laser survey, 2006.
[5] H. Nakashima *et al*, Numerical simulation of flood and inundation for the effects of Nokoshi and open levee in Jobaru River, Annual Journal of Hydraulic Engineering, JSCE, Vol.57, February,2013.